CHAPTER 13

New Materials for CO_2 Photoreduction

YONG ZHOU*[a,b], WENGUANG TU[a,b], AND ZHIGANG ZOU*[b]

[a]Key Laboratory of Modern Acoustics, MOE, Institute of Acoustics, School of Physics, Nanjing University, 22 Hankou Road, Nanjing, Jiangsu 210093, P. R. China; [b]National Laboratory of Solid State Microstructures, School of Physics, Ecomaterials and Renewable Energy Research Center (ERERC), Jiangsu Key Laboratory for Nano Technology, Nanjing University, 22 Hankou Road, Nanjing, Jiangsu 210093, P. R. China
*E-mail: zhouyong1999@nju.edu.cn, zgzou@nju.edu.cn

13.1 Introduction

It is well-established that superabundant CO_2 emission in the atmosphere is a main cause of the global warming. The atmospheric CO_2 concentration continues to rise from the ongoing burning of fossil fuels. The rapid consumption of fossil fuel and the increase of greenhouse gas emissions have brought an urgent demand for the development of renewable and clean energy sources. Several approaches have been pursued to tackle the challenges. The idea of mimicking the overall natural photosynthetic cycle of chemical conversion of CO_2 into useful fuels is gaining increasing attention.[1] The natural photosynthesis in green plants directly converts sunlight into chemical energy along with the formation of O_2 and carbohydrates from H_2O and CO_2, which produces a readily usable carbon source and an aerobic atmosphere to achieve a nature carbon neutral cycle simultaneously.

RSC Energy and Environment Series No. 14
Photocatalysis: Fundamentals and Perspectives
Edited by Jenny Schneider, Detlef Bahnemann, Jinhua Ye, Gianluca Li Puma, and Dionysios D. Dionysiou

Published by the Royal Society of Chemistry, www.rsc.org

Solar to chemical energy conversion based on artificial photosynthesis is a silver bullet solution to impact the global energy balance and greenhouse gas emissions. Solar energy is a cost-free, abundant, and reliable power supply. Earth receives about 100 000 TW of solar power at its surface, and enough energy every hour to supply humanity's energy needs for a year.[2] As one of the artificial photosynthesis technologies, photocatalytic reduction of CO_2 into hydrocarbon fuels using solar energy is one attractive approach for migrating CO_2 emission and generating useful fuels at the same time with the following advantages: (1) it could be carried out under relatively mild conditions – room temperature and pressure; (2) this process uses a mass of abandoned CO_2 as a feedstock for making fuels and chemicals driven by inexhaustible and clean solar energy; (3) the carbon neutral renewable energy and chemicals generated from CO_2 photoreduction can be stored and used when required, such as CH_4, CH_3OH, C_2H_6, and so on; (4) this technology can realize a global carbon neutral cycle *via* the reduction and/or fixation of CO_2 as carbon-neutral energy sources to support a high quality of life for eternity.

Semiconductor material, as an artificial leaf, plays an important role in the development of photocatalytic reduction of CO_2 into hydrocarbon fuels. In 1979, Inoue *et al.* initially proposed that semiconductor photocatalysts such as TiO_2, ZnO, CdS, and SiC suspended in CO_2 saturated water could photoreduce CO_2 to organic compounds such as CO, CH_4, CH_3OH, HCOOH, or others.[3] Since then, intense research has been performed on TiO_2 for CO_2 photoreduction owing to its low cost, effectiveness, nontoxicity, and chemical stability. The CO_2 photoreduction efficiency is primarily determined by the thermodynamic and kinetic balance of light-harvesting, charge carrier generation and separation, and catalytic reaction on the material surface.[4] Since photocatalysis is a surface/interface-reaction process, the rapid development of nanotechnology leads to remarkable progresses in the field of CO_2 photoreduction including the development of semiconductor materials, the design of photocatalysts with different nano-architectures, and the experimental and theoretical research into the reaction mechanism.[4,5]

Although earlier reviews generally introduce the concept of artificial photosynthesis,[6–20] this chapter begins with a brief description of the basic principles of photocatalytic reduction of CO_2 and then aims to cover state-of-the-art research activities in designing new photocatalytic materials from the point of light harvesting, adsorption of reactants, charge separation and transport, and CO_2 activation.

13.2 Basic Principles of Photocatalytic Reduction of CO_2

In terms of chemistry, the ultimate goal of photocatalysis is to drive a redox reaction with the assistance of electron–hole pairs generated by light in the presence of semiconductors, during which the excited electrons and holes serve as strong reducing agent and oxidant, respectively, to convert solar

energy into chemical energy.[21] Carbon dioxide shows no light absorption in the ultraviolet (UV)-visible region (200–800 nm). Photocatalytic reduction of CO_2 with H_2O into hydrocarbon fuels such as CH_4 and CH_3OH is an uphill reaction with a highly positive change in Gibbs free energy:

$$CO_2 + 2H_2O \rightarrow CH_3OH + 3/2O_2 \ (\Delta G^0 = 702.07 \text{ kJ mol}^{-1})$$

and:

$$CO_2 + 2H_2O \rightarrow CH_4 + 2O_2 \ (\Delta G^0 = 818.17 \text{ kJ mol}^{-1})$$

Thus, input energy is demanded to overcome these reaction barriers with the assistance of photocatalysts. Figure 13.1 depicts the basic mechanism of the photocatalytic CO_2 reduction. Firstly, under light illumination, a flux of photons absorbed by the semiconductor excites electrons from the valence band (VB) to the conduction band (CB), leaving an equal numbers of holes in the VB; secondly, the excited electrons and holes separate from each other and migrate to the semiconductor surface; finally, the electrons reduce CO_2 into hydrocarbon fuels such as CO, CH_3OH, and CH_4 in the presence of H_2O, while the holes oxidize H_2O. The overall efficiency of photocatalytic reduction of CO_2 is determined by the balance of thermodynamics and kinetics of these processes.

To achieve overall CO_2 photoreduction, the energy requirements imply that the bottom of the CB must be located at a more negative potential than CO_2 reduction potentials, while the top of the VB must be positioned at a more positive potential than H_2O oxidation potential (eqn (13.1)). Eqn (13.2)–(13.6) list the CO_2 reduction potentials *versus* the NHE at pH 7 to afford COOOH,

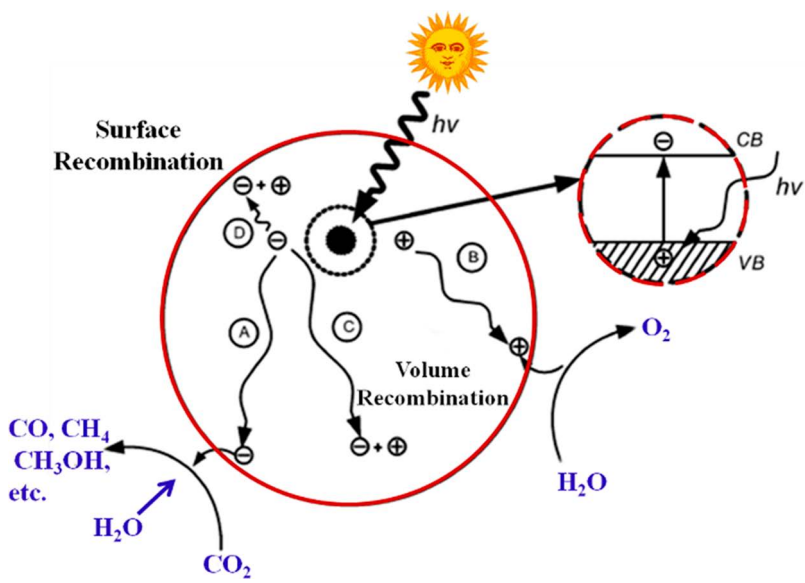

Figure 13.1 Illustration of the processes involved in CO_2 photoreduction with H_2O on the semiconductor surface.

CO, HCHO, CH_3OH, and CH_4, respectively. Obviously, a series of different products (*e.g.*, CO, CH_3OH, HCHO, and CH_4) could be formed over various photocatalysts, which is decided by the number of electrons and protons (e^-/H^+) involved in chemical reactions. Two protons and two electrons are needed in HCOOH formation, while CH_4 formation occurs by reaction with eight electrons and eight protons. The selectivity of product formation is one of the significant problems in CO_2 photoreduction process, which may be influenced by reaction conditions and thermodynamic reduction potentials:

$$H_2O \rightarrow 1/2O_2 + 2H^+ + 2e^- \quad (E^0_{redox} = 0.82\ V\ vs.\ SHE) \tag{13.1}$$

$$CO_2 + 2e^- + 2H^+ \rightarrow HCOOH \quad (E^0_{redox} = -0.61\ V\ vs.\ SHE) \tag{13.2}$$

$$CO_2 + 2e^- + 2H^+ \rightarrow CO + H_2O \quad (E^0_{redox} = -0.53\ V\ vs.\ SHE) \tag{13.3}$$

$$CO_2 + 4e^- + 4H^+ \rightarrow HCHO + H_2O \quad (E^0_{redox} = -0.48\ V\ vs.\ SHE) \tag{13.4}$$

$$CO_2 + 6e^- + 6H^+ \rightarrow CH_3OH + H_2O \quad (E^0_{redox} = -0.38\ V\ vs.\ SHE) \tag{13.5}$$

$$CO_2 + 8e^- + 8H^+ \rightarrow CH_4 + H_2O \quad (E^0_{redox} = -0.24\ V\ vs.\ SHE) \tag{13.6}$$

For any given photocatalytic material it is necessary to evaluate the efficiency of CO_2 photoreduction. The efficiency of CO_2 photoreduction is usually measured directly from the rate of production evolution, which is indicated with a unit such as μmol g^{-1} h^{-1} or ppm g^{-1} h^{-1}. Since the photocatalytic activity of CO_2 photoreduction depends on the experimental conditions such as a light source and the type of a reaction system, the activities cannot be compared with each other if the reaction conditions are different.[14,18] Moreover, it is not easy to compare the efficiency of different samples when two or more kinds of different products are obtained from CO_2 photoreduction. Therefore, it is fairer to measure the apparent quantum yield (AQY), as defined by eqn (13.7):

$$\mathrm{AQY}(\%) = \frac{\sum_i n_i m_i}{\text{Number of incident photons}} \times 100 \tag{13.7}$$

Here n_i and m_i signify the number of electrons for the generated production and the molecular number of generated production, respectively. For example, the generation of one CH_4 molecule will consume eight electrons, so $n = 8$. The solar energy conversion efficiency is usually used for evaluation of solar cells. Sometimes, the solar energy conversion efficiency (eqn (13.8)) is used for CO_2 photoreduction:

$$\text{Solar energy conversion}(\eta)(\%) = \frac{\text{Out energy of production}}{\text{Energy of incident light}} \times 100 \tag{13.8}$$

Activated CO_2 is probably an important species in photoreduced CO_2 reactions. The activation of stable CO_2 initiates multistep reactions for CO_2 reduction, which likely involves one-electron transfer to CO_2 to generate $CO_2^{\bullet-}$ species, which is the electron attached state of CO_2.[10,22,23] However, the transfer of one electron to free CO_2 is unfavorable thermodynamically, because the high LUMO level of CO_2 leads to a very negative redox potential

for this process of $CO_2 + e^- \rightarrow CO_2^{\bullet -}$ ($E^0_{redox} = -1.90$ V, *vs.* NHE), which has been proved by scanning tunneling microscopy (STM) experiments.[24,25]

It has been revealed in experiment and theoretical research that the surface sites of semiconductors play an important role in CO_2 activation, especially Ti^{3+} sites on TiO_2 surfaces and oxygen vacancy defects.[26–30] The interaction between CO_2 and surface sites of semiconductors lowers the barrier for one-electron transfer into absorbed CO_2. Oxygen vacancy defects on a TiO_2 surface are more effective for CO_2 activation than a stoichiometric TiO_2 surface.[26] The CO_2 molecules prefer to adsorb at oxygen vacancy sites with one oxygen atom of the CO_2 located at bridging oxygen vacancy defects. A missing oxygen atom would leave two extra electrons at the site of the vacancy, which reduce the adjacent two surface Ti^{4+} sites to Ti^{3+}, creating surface electron centers for the formation of the negatively charged $CO_2^{\bullet -}$ species. The Ti^{3+} sites on TiO_2 surfaces are, owing to the much higher reactivity of the charge transfer excited states, proposed to interact with absorbed CO_2 to form $CO_2^{\bullet -}$ species.[26,31]

Carbon dioxide photoreduction demands input energy to break a C=O bond and form a C–H bond, involving the participation of multiple electrons and a corresponding number of protons.[17] Methane (CH_4) is one of most obtained products during the process of photocatalytic reduction of CO_2 in the presence of H_2O vapor. Two plausible pathways for CH_4 yield are suggested:

$$(1)\ CO_2 \rightarrow CO \rightarrow C^{\bullet} \rightarrow CH_2 \rightarrow CH_4$$

and:

$$(2)\ CO_2 \rightarrow HCOOH \rightarrow HCHO \rightarrow CH_3OH \rightarrow CH_4$$

The second pathway was initially put forward by Inoue *et al.* in 1979;[3] they thought that each step in the pathways needs two electrons to take part in the chemical reactions. However, understanding of processes of CO_2 photoreduction is still in its infancy due to complex multi-electron transfer processes.

13.3 Materials for CO_2 Photoreduction

It is known that the rapid development of nanotechnology offers significant impact on the progress of semiconductor photocatalysis including the development of semiconductor materials and the design and construction of photocatalysts with different nano-architectures. Until now, developed semiconductor materials for CO_2 photoreduction include, but are not limited to, metal oxides, metal sulfides, nitrides, and phosphides.

13.3.1 Metal Oxides with d^0 and d^{10} Electronic Configurations

Most metal oxides are composed of metal cations with d^0 (Ti^{4+}, Zr^{4+}, Nb^{5+}, Ta^{5+}, V^{5+}, Mo^{6+}, W^{+6}) and d^{10} (In^{3+}, Ga^{3+}, Ge^{4+}, Sn^{4+}, Sb^{5+}) configurations; the d^0 transition metal ions have a vacant d orbital and d^{10} metal ions have a completely occupied d orbital. Figure 13.2 shows metal oxides consisting of d^0 and d^{10} metal cations as photocatalysts for CO_2 photoreduction.

The metal oxides with octahedrally coordinated d^0 electronic configuration include titanates [TiO_2,[3,10,22,32–151] $ATiO_3$ (A = Sr, Ca, Ba, Pb),[28,152–155] $K_2Ti_6O_{13}$,[156,157] $ALa_4Ti_4O_{15}$ (A = Ca, Sr, Ba)[158]], vanadates ($BiVO_4$,[159] $Fe_2V_4O_{13}$ [160]), ZrO_2,[161–164] niobates [HNb_3O_8,[165,166] $InNbO_4$,[167] $ANbO_3$ (A = Li, Na, K)[168–173]], $Bi_6Mo_2O_{15}$,[174] tantalates [Ta_2O_5,[175,176] $InTaO_4$,[177–181] $ATaO_3$ (A = Li, Na, K)[182]], and tungstates (WO_3,[183,184] $W_{18}O_{49}$,[30] Bi_2WO_6 [185,186]). The CB bottom of the d^0 binary metal oxide photocatalysts (such as TiO_2, ZrO_2, Ta_2O_5, WO_3, and so on) is usually composed of d orbitals, while the VB top consists of O 2p orbitals. The potential of VB for binary metal oxides is normally located about 3 eV *vs.* NHE,[187] which allows photogenerated holes with strong oxidation ability for H_2O oxidation thermodynamically. For partial d^0 ternary metal oxides, alkali (Li, Na, K, Rb, Cs), alkaline earth (Mg, Ca, Sr, Ba), and transition metal ions (Y, La, Gd) simply construct the crystal structure as A site cations in perovskite compounds, but do not directly contribute to the energy band structure of these compounds. For other partial d^0 ternary metal oxides, orbitals of Pb 6s in Pb^{2+} and Bi 6s in Bi^{3+} can also contribute to the formation of the VB in metal oxides, which results in an up-shift of the VB due to the positioning of low energy d or s orbitals into VB.[187]

Since 2001, Inoue's group have developed p-block metal oxides with d^{10} (In^{3+}, Ga^{3+}, Ge^{4+}, Sn^{4+}, Sb^{5+}) electronic configuration to form a group of photocatalysts for water splitting. Compared to vacant d orbital in d^0 metal ions, d^{10} metal ions have a completely occupied d orbital. Recently, d^{10} metal oxides have drawn considerable attention for CO_2 photoreduction (Figure 13.2), including $In(OH)_3$,[188] gallates (Ga_2O_3,[189–191] $ZnGa_2O_4$,[192,193] $CuGaO_2$ [194]), stannates (Zn_2SnO_4 [195]), and germinates (Zn_2GeO_4,[196–199] $In_2Ge_2O_7$ [200]). In contrast to d orbitals in the CB of d^0 metal oxides, the CB of d^{10} metal oxides consists of s and p hybrid orbitals of d^{10} metal ions, resulting in a large dispersion in k-space on the band.[201] The well dispersed bands result in high mobility of photogenerated electrons.

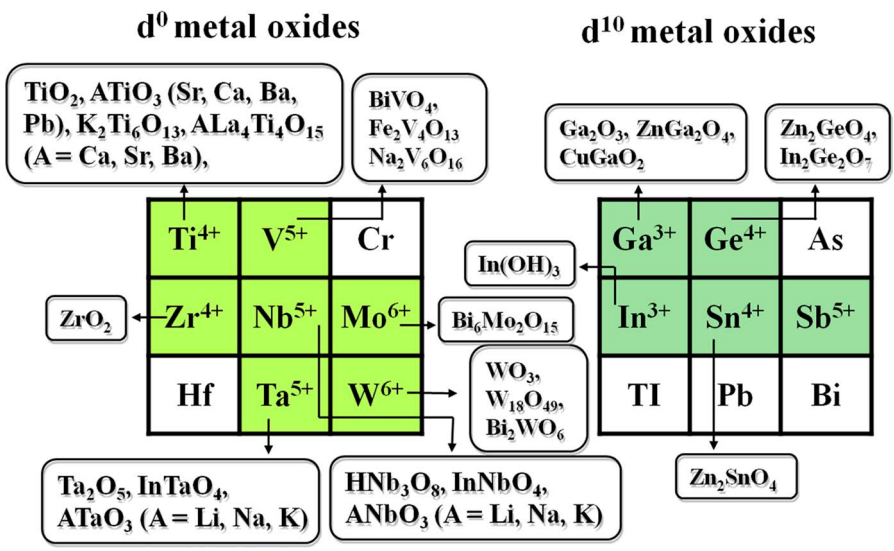

Figure 13.2 Metal oxides with d^0 (yellow) and d^{10} (green) electronic configuration as recent photocatalysts for CO_2 photoreduction.

Zn_2GeO_4 and $ZnGa_2O_4$ have been developed for CO_2 photoreduction in the last few years. The VB of Zn_2GeO_4 is formed by the hybridization of Zn 3d and O 2p orbitals. This p–d repulsion (*e.g.*, O 2p–Zn 3d) shifts the VB maximum upwards without affecting the conduction band minimum. The CB bottom of Zn_2GeO_4 is composed of the Ge 4p orbital with a small contribution of Zn 4s4p orbitals. A willemite crystal structure of Zn_2GeO_4 consists of tetrahedral GeO_4 and ZnO_4, where one tetrahedral GeO_4 and two kinds of tetrahedral ZnO_4 are combined with each other through the edge oxygen (Figure 13.3). Interestingly, the heavy distortion of GeO_4 tetrahedron generates a dipole moment of 1.6 D inside, and this local electric field is beneficial for electron–hole separation upon photoexcitation.[202] Thus, tetrahedral GeO_4 is a main unit of the photocatalytic active site, although the ZnO_4 unit influences the geometric and electronic structures of GeO_4. For $ZnGa_2O_4$, the VB is primarily derived from Zn 3d and O 2p orbitals, whereas the CB is formed by hybridization of Ga 4s4p and Zn 4s4p orbitals (Figure 13.3). A cubic structure of $ZnGa_2O_4$ is composed of GaO_6 octahedra and ZnO_4 tetrahedra. The GaO_6 octahedral unit in $ZnGa_2O_4$ also exists as a major photocatalytic active site.[203] Due to the large bandgap of Zn_2GeO_4 (4.5 eV) and $ZnGa_2O_4$ (4.4 eV), these metal oxides for CO_2 photoreduction only utilize UV light. Nitridation of Zn_2GeO_4 and $ZnGa_2O_4$ under NH_3 flow produces $(Zn_{1+x}Ge)(N_2O_x)$ and $(Ga_{1-x}Zn_x)(N_{1-x}O_x)$ solid solutions, respectively. These solid solutions possess a suitably narrow bandgap of about 2.2–2.7 eV. The VB top of these solid solutions is made up of O 2p, N 2p, and Zn 3d orbitals. The p–d repulsion of N 2p and Zn 3d orbitals raises the VB top and therefore decreases the bandgap.

13.3.2 Metal Sulfides and Phosphides

Metal sulfides such as MnS, CdS, and ZnS have been applied for CO_2 photoreduction in various solvents.[3,204–214] The CB of these binary metal sulfides is composed of d orbitals, while the VB is formed by S 3p orbitals. Since S 3p orbitals have atomic orbitals with a potential energy higher than that of O 2p orbitals, the VB of metal sulfides shifts upward compared to their oxide analogues. Thus, the CB of these binary metal sulfides has a more negative potential, which is more favorable for CO_2 photoreduction. The major

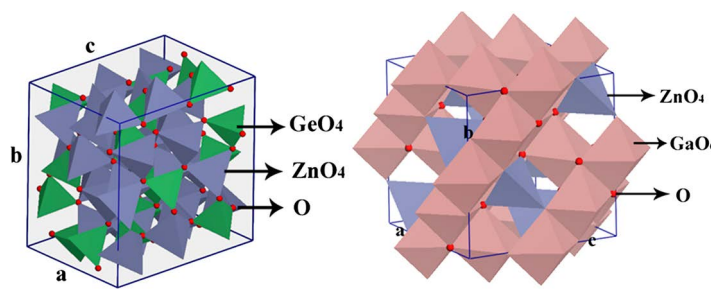

Figure 13.3 Schematic structural models of (left) Zn_2GeO_4 and (right) $ZnGa_2O_4$.

problem in CO_2 photoreduction process is that photocorrosion damages the stability of the photocatalysts under light illumination, owing to the oxidation of S^{2-} in lattices by photogenerated holes ($XS + 2h^+ \rightarrow X^{2+} + S$). However, these metal sulfides can show efficient activity for CO_2 photoreduction, when hole scavengers exist such as S^{2-}, SO_3^{2-}. The $Cu_xAg_yIn_zZn_kS$ solid solutions could undergo photocorrosion under visible light irradiation without the assistance of hole scavengers.[215] Partial metal sulfides (PbS, Bi_2S_3) with a narrow bandgap have been used as photosensitizers for CO_2 photoreduction. Cu_2ZnSnS_4 modified with a metal-complex electrocatalyst has served as photocathode for highly selective photoelectrochemical CO_2 reduction.[216]

The p-type phosphides, especially InP[217–219] and p-GaP,[220] are mainly used as photocathodes to achieve photoelectrochemical CO_2 reduction. GaP is a p-type semiconductor with a narrow band gap of 2.3 eV. One of the earliest works, reported by Halmann in 1978, achieved photoelectrochemical reduction of aqueous CO_2 by using p-type GaP cathode as a photocathode in liquid junction solar cells.[221] Recently, a p-GaP semiconductor was used as electrode in a photoelectrochemical cell to reduce CO_2 to methanol with near 100% faradic efficiency at underpotentials greater than 300 mV below the standard potential of −0.52 V *vs.* SCE in our system with a pH of 5.2.

13.3.3 Other Materials

SiC has received attention for CO_2 photoreduction, because the CB potential of SiC is more negative than those of other photocatalysts (GaP, CdS, TiO_2, WO_3), resulting in the much stronger reductive power of photogenerated electrons in SiC.[3,222,223] Recently, layered double hydroxides (LDHs) such as Zn–Al LDH,[224] Mg–In LDH,[225] and Zn–Cu–Ga LDH[224,226] have been utilized for CO_2 photoreduction. The versatility of the LDH structure allows tuning of the compositions of metal cations, charge balancing anions, and hydroxyl layer, which can adjust the adsorptive power of CO_2, tolerance of water, and active sites. However, the poor chemical stability of LDH destroys the photocatalytic performance of CO_2 photoreduction. Polymeric graphite phase carbon nitride (g-C_3N_4), as a metal-free polymeric material, is considered to be a promising visible-light-driven photocatalyst for CO_2 photoreduction, because it possesses very high thermal and chemical stability.[227,228] The surface-modified small carbon nanoparticles (average diameter ~9 nm) decorated with Au or Pt nanoparticles have showed photocatalytic activity for CO_2 photoreduction.[229]

13.4 Strategies for Designing Effective Photocatalytic Materials

Since the nature of surface/interface chemistry is one of the key issues for semiconductor photocatalysis, a series of characteristic properties of materials have a direct impact on the CO_2 conversion efficiency, including the surface area, pore structure, exposed crystal facets, surface defects, and so on.

Moreover, strategies such as cation or anion doping, solid solution formation, sensitization, and construction of heterojunction structures can tune the bandgap and band edge positions of photocatalysts. This section introduces research activities in designing new photocatalytic materials from the point of view of adsorption of reactants, light harvesting, charge separation and transport, and CO_2 activation.

13.4.1 Surface Sites for Reactant Adsorption and Chemical Reaction

The surface structure of a nanomaterial affects its physicochemical properties, such as the adsorption of reactant, susceptibility of photocatalyst toward photocorrosion, and surface energy. The surface area, pore structure, exposed crystal facets, and surface defects show significant impact on the activity of CO_2 photoreduction.

13.4.1.1 Porous Structure with Large Surface Area

A large surface area can increase the adsorption of reactants (*e.g.*, CO_2, H_2O) and also supply abundant surface active sites for chemical reaction. According to an IUPAC definition, porous materials are classified into three major categories depending on their pore sizes: microporous materials with pore sizes below 2 nm, mesoporous materials with pore sizes between 2 and 50 nm, and macroporous materials with pore sizes exceeding 50 nm. Micro/mesoporous nanomaterials have attracted considerable attention in the field of CO_2 photoreduction, due to the specific surface area, ordered pore structure, and readily accessed channels.

To date, a limited number of routes including evaporation-induced self-assembly and nonaqueous solvent methods have been developed to synthesize mesoporous metal oxides. In these routes, surfactant molecules or a template is generally introduced to construct mesoporous structures. Maintaining mesoporous structures during removal of the templates is a key process for obtaining the expected structures. Ordered mesoporous CeO_2–TiO_2 composites with 2D hexagonal structure and hierarchical porosity for CO_2 photoreduction were synthesized through evaporation-induced self-assembly using ordered mesoporous SBA-15 as template.[110]

Natural leaves have demonstrated the perfect assembly of hierarchical levels of porosity into 3D elaborated architectures with high porosity, high connectivity, and high surface area. Ye *et al.* utilized the 3D hierarchical architecture of a leaf as an ideal parent template to fabricate perovskite titanates ($ATiO_3$, A = Sr, Ca, and Pb) with hierarchical anatomy from macro- to nanoscales for CO_2 photoreduction (Figure 13.4).[154] This method converts the morphological elements of the natural photosynthetic system into artificial photosynthetic system, including: (1) unique 3D architecture for enhanced light harvesting; (2) efficient mass flow network with 3D multiple-scaled

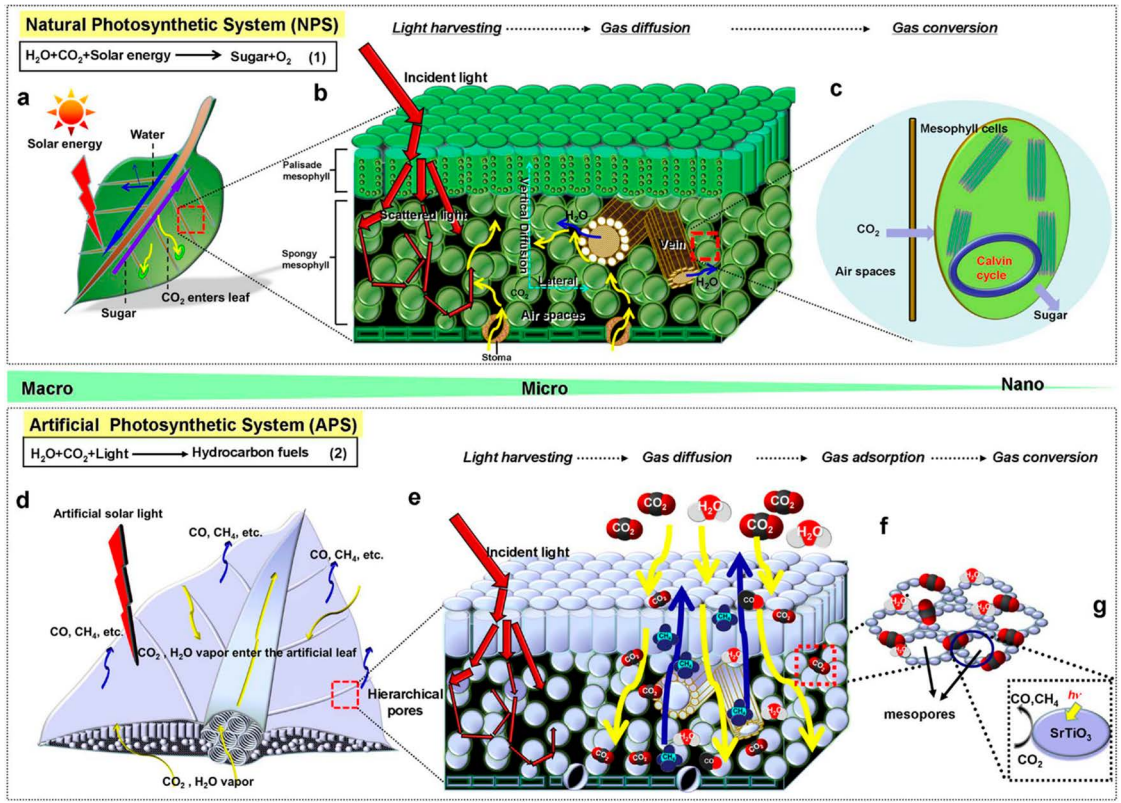

Figure 13.4 Schematic illustration and comparison of the key processes in a natural photosynthetic system (NPS) and an artificial photosynthetic system (APS). (a) Basic process of photosynthesis in NPS at the macroscale. (b) Light harvesting and gas diffusion processes in NPS at the microscale. (c) Gas conversion process in mesophyll cells at the nanoscale. (d) Basic process of artificial photosynthesis in APS at the macroscale. (e) Light harvesting and gas diffusion processes in APS at the microscale. (f) Gas adsorption process in APS at the nanoscale. (g) Gas conversion process in APS at the nanoscale.[154]

hierarchical porosity to suffer minimum gas diffusion; and (3) high surface areas for improved overall reaction performances. This general method for the construction of 3D architectures of perovskite titanates ($ATiO_3$, A = Sr, Ca, and Pb) can be extended to other multi-metallic oxides. A series of alkaline tantalates ($MTaO_3$, M = Li, Na, K) with hierarchical porous anatomy for CO_2 photoreduction were fabricated using activated carbonized tree trunks as templates.[230] Mesoporous β-Ga_2O_3 with an average pore size of 3.8 nm realized enhanced activity for CO_2 photoreduction into CO and CH_4 compared with that of commercial β-Ga_2O_3, due to higher surface area and mesoporous channels for efficient CO_2 adsorption.[190]

Metal–organic frameworks (MOFs) are a class of crystalline micro/mesoporous hybrid materials with an extended 3D network, which is constructed by metal ions or small discrete clusters through the linkage of multidentate organic molecules.[171] Zeolitic imidazolate frameworks (ZIFs), as a type of MOF, have excellent chemical and thermal stability, and structural stability in water. Zn_2GeO_4/ZIF-8 hybrid nanorods containing 25 wt% ZIF-8 exhibited 3.8-times higher dissolved CO_2 adsorption capacity than bare Zn_2GeO_4 nanorods, resulting in a 62% enhancement in CO_2 photoreduction into liquid CH_3OH fuel.

In recent years, a simplified soft-chemistry route based on a reactive template has been developed to allow the synthesis of pure mesoporous semiconductors to proceed at room temperature without requiring the introduction or removal of a template. Mesoporous $ZnGa_2O_4$ with a wormhole framework was prepared by an ion-exchange reaction at room temperature involving a mesoporous $NaGaO_2$ colloid precursor, which does not require the introduction of morphology controlling agents.[192] Significantly, this method can be extended to prepare $ZnGa_2O_4$ nanocubes[193] and other porous materials, such as $CoGa_2O_4$,[192] $NiGa_2O_4$,[192] Zn_2GeO_4,[198,231] zinc gallogermanate solid solution,[232] and Bi_2WO_6.[186] Mesoporous $ZnGa_2O_4$ with 1 wt% RuO_2 co-catalyst showed higher activity for CO_2 photoreduction into CH_4 than that obtained by solid-state reaction (ss-$ZnGa_2O_4$), owing to strong gas adsorption by the mesostructure and more reaction sites arising from a high specific surface area.[192]

13.4.1.2 Optimized Surface Reactivity via *Facet Engineering*

The photocatalytic activity and selectivity of semiconductors are inherently determined by the surface atomic structure tuned *via* crystal facet engineering, because the surface atomic arrangement and coordination affect physicochemical properties of semiconductors such as surface energy, surface active site, and electronic band structure.[233] Due to the minimization of surface energy during crystal growth, anatase TiO_2 under equilibrium conditions is dominated by the thermodynamically stable {101} facets (up to 94%) and few {001} facets, no {100} facet will appear, owing to the Wulff construction and theoretically calculated surface energy ({101} (0.44 J m^{-2}) < {100} (0.53 J m^{-2}) < {001} (0.90 J m^{-2})).[234,235] Anatase TiO_2 crystals with ~47% exposed {001} facets were fabricated using hydrofluoric acid (HF) as morphology controlling

agent.[236] It revealed that the formation of high F–Ti bonding energy significantly lowers the energy of the (001) surfaces, making them more stable than (101) surfaces in the reaction media. The yield of CH_3OH formation was much higher on TiO_2 (100) than on TiO_2 (110), while the formation of CH_4 was only observed on TiO_2 (100) and not on TiO_2 (110), revealing that the exposed crystal facets play important role in photocatalytic reactivity and selectivity.[237,238] Hollow anatase TiO_2 single crystals with dominant {101} facets featuring the use of F^-/PO_4^{3-} as morphology controlling agent showed improved activity for photoreduction of CO_2 into CH_4 compared with solid anatase TiO_2 single crystals, due to shortened diffusion length of carriers and increased surface area.[98] The {100} facets have 100% five-coordinated Ti (Ti_{5c}) atoms in contrast to {101} facets with only 50% Ti_{5c} atoms, because Ti_{5c} atoms can act as active sites in the photocatalytic reaction.[233] TiO_2 ultrathin nanosheets with 95% of exposed {100} facet exhibited significantly higher photocatalytic activity for reduction of CO_2 into CH_4 compared with TiO_2 cuboids with 53% of exposed {100} facet, because the higher percentage of exposed {100} facets and larger surface area offer more active sites (Ti_{5c} atoms) in the photocatalytic reaction.[111] A {010} with a surface energy of 0.53 J m^{-2} has the same 100% Ti_{5c} atoms as {100}.[89] Theoretically, H_2O molecules at low coverage can be dissociatively adsorbed on the (010) surface with 100% Ti_{5c} atoms, while the H_2O molecules can only be molecularly adsorbed on (101).[239] Furthermore, the interaction of CO_2 on the (010) is predicted to be stronger than that on both (101) and (001).[240] Therefore, acquiring a high percentage of {010} facets is of great significance in optimizing the photocatalytic activity of anatase TiO_2. Single crystalline anatase TiO_2 rods with dominant reactive {010} facets showed a superior photocatalytic conversion of CO_2 into CH_4 compared to benchmark P25 TiO_2 nanocrystals.[89]

Recently, $ZnGa_2O_4$ nanocubes with {100} facets were prepared *via* an ion-exchange process using the GaOOH single crystal nanoplate as a precursor without requiring the introduction of morphology controlling agents.[193] $ZnGa_2O_4$ nanocubes with exposed {100} facets exhibited improved performance in the photocatalytic reduction of CO_2 into CH_4 under UV-vis light irradiation, compared with mesoporous $ZnGa_2O_4$ that has a larger specific surface area than that of $ZnGa_2O_4$ nanocubes. Theoretical calculations indicates that the light-hole effective mass on the {100} facets of $ZnGa_2O_4$ corresponds to the high hole mobility, which contributes to efficient H_2O oxidation to offer the protons for promoting CO_2 reduction into CH_4. Single crystal Zn_2GeO_4 nanorods with dominant (110) crystal face were also prepared by an ion-exchange process of mixing Na_2GeO_3 and $Zn(CH_3COO)_2$ solutions, which exhibited improved photocatalytic activity for CO_2 reduction, owing to the high specific surface area and dominant (110) crystal facet.[197]

Exposed facet engineering can adjust the electronic band structures of semiconductors.[183–185] A single-crystal WO_3 ultrathin nanosheet ~4–5 nm thick, corresponding to six repeating unit cells of monoclinic WO_3 along the *c*-axis, was synthesized with laterally oriented attachment of tiny WO_3 nanocrystals formed using a solid–liquid phase arc discharge route in an aqueous

solution.[183] In accordance with the reported dimensions, no quantum confinement is expected in the lateral direction, whereas the structures should be strongly confined vertically due to their extremely small thickness. This WO_3 ultrathin nanosheets with dominantly exposed {001} facets exhibited enhanced performance for photocatalytic reduction of CO_2 into CH_4 under visible light irradiation, because size-quantization effects in this ultrathin nanostructure alter the WO_3 band gap. Moreover, theoretical calculations indicate that exposure of the {001} crystalline facet of the well-defined Bi_2WO_6 nanoplate gives a particularly reactive surface energetically favoring the reduction of CO_2.[185]

13.4.1.3 Surface Modification

Because photocatalytic redox reactions take place on the surface, modification of the semiconductor surface can affect the physicochemical properties for the CO_2 photoreduction. The surface chemistry of CO_2 demonstrated that adsorption of CO_2 molecules on the semiconductor surface is usually accompanied with activation processes. Compared with the normal molecule, CO_2 in a chemisorbed state (mainly carbonate and/or CO^{2-} anion) has a lower LUMO level with a bent O–C–O bond angle, which favors charge transfer from photo-excited semiconductors to the adsorbed CO_2 molecules.[10] The nonlinear CO_2 molecules generated on the surface of solid bases are more destabilized than the linear CO_2 molecules, showing high reactivity for CO_2 photoreduction. Amine groups on the semiconductor surfaces can promote CO_2 capture, because the chemical interactions between amine groups and CO_2 result in formation of carbamate (or bicarbamate) that can transform into carbonate upon hydrolysis. Amine-functionalized TiO_2 nanoparticles were prepared by a simple solvothermal process with monoethanolamine and $TiCl_4$ as starting materials; these nanoparticles show substantially increased affinity for CO_2 on TiO_2 surfaces for more effective CO_2 activation.[241] The amine groups enable C–N bonding with CO_2 to form activated CO_2 molecules and efficient charge transfer between CO_2 molecules and TiO_2, significantly enhancing the photocatalytic rate of CO_2 reduction into CO and CH_4. Similarly, surface modification of TiO_2 with NaOH was found to be an effective way for CO_2 adsorption, activation, and high efficiency for CO_2 photoreduction into CH_4.[149] Optimized loading of NaOH kept a good balance between CO_2 chemisorption quantity and BET surface area of TiO_2.

A thin Nafion overlayer on Pd–TiO_2 significantly increased photocatalytic activity for CO_2 reduction into CH_4 and C_2H_6 under UV and solar light.[99] The Nafion layer enhances the local proton activity within the layer to facilitate multi-electron transfer reactions, during which the production of C_2H_6 requires even more protons and electrons than that of CH_4. Moreover, various intermediates involved in the formation of C_2H_6 can be stabilized in the Nafion layer and the re-oxidation of CO_2 reduction products could be inhibited.

13.4.1.4 Surface Oxygen Vacancy

Oxygen vacancy defects play an important role in the adsorption and activation of CO_2 (as discussed in Section 13.2). Recently, ultrathin $W_{18}O_{49}$ nanowires (0.9 nm in diameter) with a large number of oxygen vacancies were prepared by a very simple one-pot solution-phase method, which showed strong light absorption from the visible to the near-infrared region.[30] Oxygen vacancy-rich ultrathin $W_{18}O_{49}$ nanowires showed an excellent capability of selective reduction of CO_2 into CH_4 under visible light irradiation ($\lambda > 420$ nm) because oxygen vacancies provide reductive sites for CO_2 adsorption and reduction. Oxygen vacancies were fully consumed after irradiation for 90 h, but could be easily recovered by utilizing the strong reducing power of $NaBH_4$. Self-doped $SrTiO_{3-\delta}$ upon treatment in Ar at temperatures from 1200 to 1400 °C showed increasing photocatalytic activity for CO_2 reduction under visible light irradiation ($\lambda > 420$ nm), due to the increasing concentration of surface oxide vacancies with increasing heating treatment.[28] The oxygen vacancies and Ti^{3+} together induce an in-gap band to enhance visible light absorption. The sample at 1300 °C realized the highest photocatalytic activity for CO_2 reduction with a quantum efficiency of 0.21% at 600 nm. Higher temperature treatment, at 1400 °C, damaged the photocatalytic activity, owing to the disorder of atom arrangement and the loss of crystallinity at the relatively high temperature. Similar phenomenon for CO_2 reduction was observed over monoclinic phase $Bi_6Mo_2O_{15}$ microwires (20–60 μm long, 200–400 nm in diameter) with post-heating treatment at different temperatures.[174] The surface oxide vacancies can greatly prolong the lifetime of photoexcited carriers for efficient electron–hole separation.

13.4.2 Light Harvesting for Effectively Utilizing Solar Energy

The energy band configuration of semiconductors plays a significant role in the absorption of light. Bandgap engineering is an effective approach to adjust band position and bandgap for effectively utilizing solar energy, including cation or anion doping, solid solution formation, and sensitization.

13.4.2.1 Ion Doping

As the VB potential of developed metal oxide photocatalysts is normally located about 3 eV *vs.* NHE, these metal oxide photocatalysts only utilize UV light.[187] Doping with anions such as N and C is an effective strategy to raise the VB maxima and narrow the bandgap of metal oxides so as to extend the absorbed light range. TiO_2 is one of most effective semiconductors for CO_2 photoreduction, due to its nontoxicity, low cost, and chemical stability. However, a large bandgap (3.2 eV) of anatase TiO_2 utilizes only about 3–5% of solar spectrum. N-doped TiO_2 showed high activity for CO_2 photoreduction under visible light irradiation ($\lambda > 420$ nm).[135] The mixing of N 2p orbitals

with O 2p orbitals results in up-shift of VB, leading to bandgap narrowing and visible absorption. N-doped $InTaO_4$ with Ni@NiO core–shell nanostructure as co-catalyst was prepared for photocatalytic reduction of CO_2 with H_2O into CH_3OH under light irradiation (λ ranges from 390 to 770 nm).[181] Orthorhombic Ta_2O_5, an n-type semiconductor, has a wide band gap of 4.0 eV. Interestingly, nitrogen doping in Ta_2O_5 not only caused a redshift of 200 nm at the absorption edge of Ta_2O_5 but it also provides p-type conductivity in N-doped Ta_2O_5.[175,176] N-doped Ta_2O_5 linked with Ru complex electrocatalysts showed selective conversion of CO_2 into HCOOH under visible light irradiation ($410 < \lambda < 750$ nm).

Doping cations into the lattices of TiO_2 can create impurity energy levels within the band gap. The behavior of charge carriers such as interfacial electron transfer rate and the recombination rate is significantly influenced by doping cations.[242] Cerium-doped TiO_2 showed a redshift in the range 400–500 nm, which contributes to enhanced activity for CO_2 photoreduction.[144] However, higher Ce concentration destroyed activity for CO_2 photoreduction, owing to the formation of recombination centers by excess Ce. The yield of CH_4 and CH_3OH over Ag-doped TiO_2 (1–7 wt% Ag) was caused by two mechanisms: Ag doping in TiO_2 (up to 5 wt%) resulted in the shift of absorption edge towards visible light and increased generation of electron–hole pairs, and when Ag content was above 5 wt% the formation of a Schottky barrier at the metal–semiconductor interface around Ag metallic clusters enhanced electron–hole separation.[122]

13.4.2.2 Solid Solutions

In 2006, $(Ga_{1-x}Zn_x)(N_{1-x}O_x)$ solid solution modified with nanoparticles of a mixed oxide of rhodium and chromium was developed for overall splitting of water under visible light with a quantum efficiency of 2.5% at 420–440 nm.[243] Yellow $Zn_{1.7}GeN_{1.8}O$ solid solution (2.6 eV) was obtained through nitriding Zn_2GeO_4 crystals with sheaf-like hyperbranched nano-architectures, which showed a substantially smaller bandgap than that of the Zn_2GeO_4 precursor (4.5 eV).[244] The visible-light response of $Zn_{1.7}GeN_{1.8}O$ originates from p–d repulsion of N 2p and Zn 3d orbitals, which lifts the VB top and thus narrows the bandgap. $Zn_{1.7}GeN_{1.8}O$ with 1 wt% Pt and 1 wt% RuO_2 co-catalysts exhibited the highest activity for CO_2 photoreduction with an apparent quantum yield of 0.024% at a wavelength of 420 ± 15 nm. Zinc gallogermanate solid solution (denoted as $4.5(ZnGa_2O_4)$:(Zn_2GeO_4)) was successfully synthesized through a hydrothermal ion exchange reaction.[232] Introduction of Zn_2GeO_4 into $ZnGa_2O_4$ can effectively narrow the bandgap by an upshift of VB edge from the enhanced p–d (O 2p–Zn 3d) repulsion effect *via* incorporation of s and p orbitals of Ge, and the downshift of CB edge through introducing the low-energy s orbital of Ge. The zinc gallogermanate solid solution also possesses a light-hole effective mass with high mobility and thus enhances the ability of the photocatalyst in water oxidation to provide protons for CO_2 photoreduction.

13.4.2.3 Sensitization

Sensitizing wide-bandgap semiconductors with dye molecules or narrow-bandgap semiconductors is an effective approach to realize visible CO_2 photoreduction. Both CdS- and Bi_2S_3-sensitized TiO_2 nanotubes showed high activity for CO_2 photoreduction into CH_3OH using Na_2SO_3 as a hole scavenger under visible light irradiation.[134] Photogenerated holes react with adsorbed H_2O molecules on a AgBr/TiO_2 catalyst surface to form $^{\bullet}OH$ radicals and H^+, which will benefit the generation of CH_4 and CH_3OH under visible light irradiation ($\lambda > 420$ nm).[125] The yields of CO, CH_4, and C_2H_6 were detected over PbS QDs sensitized TiO_2 with Cu co-catalyst.[129] However, the photocatalysts became inactive after 8 h of continuous visible light irradiation due to the photo-oxidation of PbS QDs.

Dye molecules have also been coupled with TiO_2 for CO_2 photoreduction under visible light irradiation.[116–121,124,130,141,142,146] $[Ru(Bpy)_3]^{2+}$ dye sensitized TiO_2 films showed efficient activity for CO_2 photoreduction into CH_4 under visible light irradiation, owing to the generation of catalytically active electrons from organic dye to TiO_2.[117,118] The hybrid system consisting of a ruthenium bipyridyl sensitizer (RuP) and TiO_2 functionalized with the enzyme CODH was developed for CO_2 photoreduction into CO under visible light irradiation.[124,130] RuP dyes transfer electrons into the CB of TiO_2, and these electrons are injected into CODH and the active sites where CO_2 is reduced to CO. The dye could be regenerated by a sacrificial electron donor of 2-(*N*-morpholino)ethanesulfonic acid. An air-stable copper(I) dye sensitized TiO_2 exhibited efficient light harvesting and high efficiency for CO_2 photoreduction into CH_4 under visible light irradiation ($\lambda > 420$ nm).[142] Cobalt-phthalocyanine (CoPc) dye[116,120,121] or zinc-phthalocyanine (ZnPc) dye[141] has been linked with TiO_2 for CO_2 photoreduction in NaOH solution containing Na_2SO_3 as a hole scavenger.

13.4.3 Charge Separation for Effectively Utilizing Solar Energy

During photocatalytic process, electron–hole pairs separate effectively from each other and arrive at the semiconductor surface, minimizing the recombination of electron–hole pairs and thus resulting in efficient performance of CO_2 photoreduction.

13.4.3.1 Loading Co-Catalysts

Loading appropriate co-catalysts such as metals (Pt, Rh, Pd, Cu, Ag, and Au) and metal oxides (NiO and RuO_2) on semiconductor surfaces can enhance the efficiency of CO_2 photoreduction. As shown in Figure 13.5, metals (Pt, Rh, Pd, Cu, Ag, and Au) and NiO could act as reduction sites whereas metal oxides (RuO_2, IrO_2, and CoO_x) are oxidation sites.[245,246] Co-catalysts could promote the separation and migration of photogenerated charge

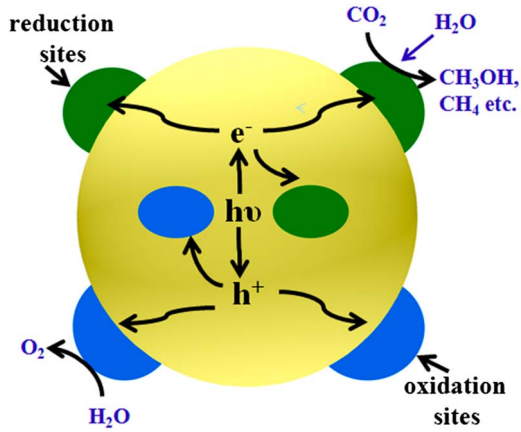

Figure 13.5 Illustration of semiconductor with co-catalysts (Pt, Rh, Pd, Cu, Ag, Au, and NiO) as reduction sites or co-catalysts (RuO_2, IrO_2, and CoO_x) as oxidation sites for CO_2 photoreduction with H_2O.

carriers to inhibit the electron–hole recombination, due to the form of an internal electric field between semiconductors and co-catalysts.

Electron transfer from semiconductors to metals is feasible thermodynamically, because the Fermi level of the metals normally lies below the CB edge of semiconductors. Deposition of a series of 2 wt% metals (Pt, Rh, Pd, Cu, Ru, and Au) on TiO_2 considerably accelerated CO_2 photoreduction into CH_4 and/or acetic acid.[34] TiO_2 with Pt or Pd mainly produced CH_4, but a considerable amount of acetic acid was produced using other metal loaded TiO_2. A TiO_2 1D film with ultrafine Pt nanoparticles (1.04 ± 0.08 nm) exhibited the highest performance for CO_2 photoreduction into CH_4.[104] It is proposed that the smaller Pt nanoparticles possess a higher Fermi level due to quantum confinement, preventing electron transfer from CB of TiO_2 to Pt, and the properties of bigger Pt nanoparticles may approach that of bulk Pt, capturing both photoelectrons and holes and acting as recombination centers. Co-loading RuO_2 and Pd on TiO_2 apparently enhanced activity for CO_2 photoreduction, because photogenerated electrons transfer from TiO_2 to Pd sites to promote the reduction of CO_2 to $HCOO^-$ and photogenerated holes inject into the RuO_2 site to accelerate the oxidation of SO_3^{2-} to SO_4^{2-}.[57] The perovskite $BaLa_4Ti_4O_{15}$ with Ag co-catalyst on the edge exhibited high activity for CO_2 photoreduction into CO.[158] The basal plane of $BaLa_4Ti_4O_{15}$ is the oxidation site for water splitting, while the edge is the reduction site. The separation of reaction sites could suppress back reactions such as oxidation of formed CO.

$InTaO_4$ with NiO co-catalyst exhibited a steady rate of CH_3OH production of 11.1 μmol g^{-1} h^{-1}, because the formation of a Schottky barrier at the surfaces traps electrons and suppress the electron–hole recombination. To effectively extract photogenerated electrons to surfaces, a core–shell structure of metallic Ni core and NiO shell (denoted as Ni@NiO) was formed on

the surface of $InTaO_4$ through reduction–oxidation pretreatment.[177] The Ni core benefits the transport of photogenerated electrons to NiO shell surfaces while the NiO shell offers active sites to react with absorbed CO_2. A similar core–shell-structured Pt@Cu_2O co-catalyst on TiO_2 was also designed to promote photoreduction of CO_2 with H_2O into CH_4 and CO.[112] Moreover, the deposition of a Cu_2O shell on Pt markedly suppresses the reduction of H_2O to H_2, a competitive reaction with the reduction of CO_2.

In addition to appropriate metals and metal oxides, carbon materials such as carbon nanotubes (CNTs) and graphene can also act as electron transporter and acceptor to efficiently reduce electron–hole recombination, playing the role of co-catalyst for CO_2 photoreduction. CNT@Ni-doped TiO_2 displayed higher activity for CO_2 photoreduction into CH_4 than that of Ni-doped TiO_2 under visible light irradiation, mainly owing to the electron transfer from TiO_2 to CNTs through d–π conjugation between TiO_2 and CNT.[145] Graphene is a zero bandgap semiconductor, possessing unique electrical properties such as massless fermions, ballistic electronic transport, and ultrahigh electron mobility.[247] Robust hollow spheres consisting of $Ti_{0.91}O_2$ nanosheets and graphene nanosheets showed higher enhancement for CO_2 photoreduction into dominant CO and minor CH_4 than that of commercial P25, due to (1) the ultrathin nature of $Ti_{0.91}O_2$ nanosheets, which allows charge carriers to transfer rapidly onto the surface for redox reaction; (2) the compact contact of $Ti_{0.91}O_2$ nanosheets with graphene nanosheets, which allows photogenerated electrons to move rapidly from $Ti_{0.91}O_2$ nanosheets to graphene to the prolong lifetime of the charge carriers; (3) the hollow structure, which potentially enhances light absorption *via* the multi-scattering of incidence light.[102] Graphene–TiO_2 hybrid nanosheets exhibited high and selective activity for CO_2 photoreduction into CH_4 and C_2H_6, owing to the electron transfer from TiO_2 to grapheme *via* Ti–O–C.[109] The synergistic effect of graphene and the surface-Ti^{3+} sites benefits the generation of C_2H_6, and the yield of C_2H_6 increased with the content of incorporated graphene. The influence of defect densities of graphene on CO_2 photoreduction was investigated by preparing graphene–P25 nanocomposite thin films through two major solution-based pathways, oxidation reduction and solvent exfoliation.[88] The improved electrical mobility of the less defective graphene allows photoexcited electrons to more effectively diffuse to reactive sites, facilitating photoreduction reactions.

13.4.3.2 One-Dimensional Nanostructures

One-dimensional nanostructures provide a direct pathway for electron transport, which should be beneficial for electron–hole separation. Nitrogen-doped TiO_2 nanotube arrays up to 130 μm in length with Cu and Pt nanoparticles as co-catalysts showed an enhanced activity for CO_2 photoreduction.[81] It was revealed that the hole and electron diffusion lengths in TiO_2 nanotube arrays are about 10 nm and 10 μm, respectively, while half nanotube wall thickness is approximately 10 nm. Single-crystalline Zn_2GeO_4 nanobelts that were hundreds of micrometers long, 20–50 nm wide, and as

thin as ~7 nm (corresponding to five repeating cell units) exhibited efficient activity for CO_2 photoreduction.[196] The ultralong longitudinal dimension provides a sufficiently spacious transport channel for charge separation and transportation. One-dimensional $Fe_2V_4O_{13}$ nanoribbons 300–400 nm wide, 20–30 nm thick, and 10–20 μm long were directly grown on a stainless-steel mesh (SSM) by a simple and facile hydrothermal approach without surfactants or templates.[160] $Fe_2V_4O_{13}$ nanoribbons with a bandgap of 1.83 eV also served as a new candidate for CO_2 photoreduction into CH_4 under visible light irradiation. Growing a 1D nanostructure directly on substrates avoids the complex recycling process of powders from solution when CO_2 photoreduction is carried in aqueous systems.

13.4.3.3 Heterojunction Construction

The type II semiconductor heterostructure is one of the most typical heterostructures that promotes spatial electron–hole separation *via* transferring photoexcited electrons in the higher CB to the lower CB and holes in the lower VB to the higher VB. Well-defined homogeneously hybrid TiO_2 mesoporous "French fries" (TiO_2/ZnO, TiO_2/Fe_2O_3, TiO_2/CuO, TiO_2/NiO, TiO_2/Cr_2O_3, and TiO_2/CeO_2) with high specific surface area, large pore volume, and pore walls were prepared by a furfural alcohol-derived polymerization–oxidation route.[94] TiO_2/ZnO exhibited higher enhancement for CO_2 photoreduction into CH_4, mainly because electrons in the CB of ZnO (−0.31 V) transfer to the CB of TiO_2 (−0.29 V) and holes in the VB of TiO_2 transfer to the VB of ZnO.

TiO_2 exhibits three crystalline polymorphs in nature: anatase, rutile, and brookite. Rutile TiO_2 nanoparticle modified anatase TiO_2 nanorods with exposed {010} facets showed higher activity for CO_2 photoreduction into CH_4 than that of pure anatase TiO_2 nanorods, due to the transfer of electrons from anatase TiO_2 to rutile TiO_2.[103] TiO_2 consisting of anatase and brookite exhibited remarkable performance for CO_2 photoreduction into CH_3OH, which was assigned to the transfer of electrons from brookite TiO_2 to anatase TiO_2.[139]

13.4.3.4 Z-Scheme CO_2 Reduction

The artificial Z-scheme system inspired by natural photosynthesis in green plants has been employed for CO_2 photoreduction.[218,219,248] The artificial Z-scheme photocatalytic system uses two different semiconductor photocatalysts with reversible redox mediators driven by a two-step photoexcitation, keeping holes/electrons with stronger oxidation/reduction abilities on different active sites (Figure 13.6). Ishitani *et al.* synthesized a visible-light-driven Z-scheme consisting of a Ru(II) dinuclear complex (RuBLRu′) for CO_2 reduction and Ag-loaded TaON for methanol oxidation under visible light irradiation (λ > 400 nm).[248] Isotope experiments clearly showed that this hybrid photocatalyst mainly produced HCOOH from CO_2 and HCHO from methanol, converting solar energy into chemical energy with a positive change in Gibbs energy of 83.0 kJ mol^{-1}.

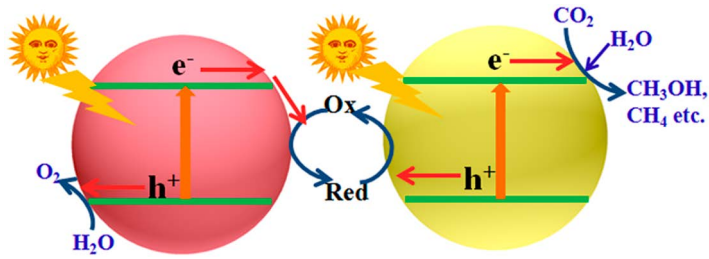

Figure 13.6 Illustration of a Z-scheme system (two-step photoexcitation system) for CO_2 photoreduction with H_2O.

13.5 Conclusions and Perspectives

In this chapter, we demonstrates a clear phenomenon, namely, that the development of materials offers increasing opportunities in the field of CO_2 photoreduction into hydrocarbon fuels using abundant solar energy in terms of (1) a large surface area for molecular adsorption and chemical reaction, (2) adjusting of band position and bandgap for effective utilization of solar energy, and (3) effective charge separation and transfer for a chemical reaction. The development of nanotechnology allows us to design and fabricate new photocatalytic materials to match the breakthrough in photocatalytic efficiency, such as d^{10} metal oxides or oxynitrides ($ZnGa_2O_4$, Zn_2SnO_4, Zn_2GeO_4, $(Zn_{1.44}Ge)(N_{2.08}O_{0.38})$, ZnGaNO). It is of great importance to explore possible cost-effective approaches for constructing nanomaterials for the photocatalytic reduction of CO_2. The present goal is to synthesize photoactive materials able to chemically couple these light driven redox reactions together and achieve conversion efficiency and selectivity that exceeds nature's photosynthesis. It is also needs to be founded on photoactive materials made of earth abundant, non-toxic, light-stable, scalable and low-cost materials.

The quantum yield of CO_2 photoreduction is still lower than that of natural photosynthesis. Strategies used to improve the efficiency include the exploration of novel photocatalytic materials, tracing the photocatalytic process through *in situ* observations, and an understanding of the mechanism *via* experimental analysis and theoretical calculations. It is sincerely hoped that the multiple collaborations for this rapidly evolving field can provide the breakthrough in overall efficiency leading to commercialization and industrialization in a way that is cost-competitive with fossil fuels.

References

1. A. Listorti, J. Durrant and J. Barber, *Nat. Mater.*, 2009, **8**, 929.
2. Q. Schiermeier, J. Tollefson, T. Scully, A. Witze and O. Morton, *Nature*, 2008, **454**, 816.
3. T. Inoue, A. Fujishima, S. Konishi and K. Honda, *Nature*, 1979, **277**, 637.

4. W. G. Tu, Y. Zhou and Z. G. Zou, *Adv. Mater.*, 2014, **26**, 4607.
5. H. Tong, S. X. Ouyang, Y. P. Bi, N. Umezawa, M. Oshikiri and J. H. Ye, *Adv. Mater.*, 2012, **24**, 229.
6. H. Yoneyama, *Catal. Today*, 1997, **39**, 169.
7. P. Usubharatana, D. McMartin, A. Veawab and P. Tontiwachwuthikul, *Ind. Eng. Chem. Res.*, 2006, **45**, 2558.
8. G. R. Dey, *J. Nat. Gas Chem.*, 2007, **16**, 217.
9. K. Koci, L. Obalova and Z. Lacny, *Chem. Pap.*, 2008, **62**, 1.
10. V. P. Indrakanti, J. D. Kubicki and H. H. Schobert, *Energy Environ. Sci.*, 2009, **2**, 745.
11. S. C. Roy, O. K. Varghese, M. Paulose and C. A. Grimes, *ACS Nano*, 2010, **4**, 1259.
12. M. R. Hoffmann, J. A. Moss and M. M. Baum, *Dalton Trans.*, 2011, **40**, 5151.
13. A. Dhakshinamoorthy, S. Navalon, A. Corma and H. Garcia, *Energy Environ. Sci.*, 2012, **5**, 9217.
14. G. H. Liu, N. Hoivik, K. Y. Wang and H. Jakobsen, *Sol. Energy Mater. Sol. Cells*, 2012, **105**, 53.
15. K. Mori, H. Yamashita and M. Anpo, *RSC Adv.*, 2012, **2**, 3165.
16. W. Q. Fan, Q. H. Zhang and Y. Wang, *Phys. Chem. Chem. Phys.*, 2013, **15**, 2632.
17. S. N. Habisreutinger, L. Schmidt-Mende and J. K. Stolarczyk, *Angew. Chem., Int. Ed.*, 2013, **52**, 7372.
18. Y. Izumi, *Coord. Chem. Rev.*, 2013, **257**, 171.
19. V. Jeyalakshmi, K. Rajalakshmi, R. Mahalakshmy, K. R. Krishnamurthy and B. Viswanathan, *Res. Chem. Intermed.*, 2013, **39**, 2565.
20. S. Navalon, A. Dhakshinamoorthy, M. Alvaro and H. Garcia, *ChemSusChem*, 2013, **6**, 562.
21. A. L. Linsebigler, G. Q. Lu and J. T. Yates, *Chem. Rev.*, 1995, **95**, 735.
22. J. Rasko and F. Solymosi, *J. Phys. Chem.*, 1994, **98**, 7147.
23. N. M. Dimitrijevic, B. K. Vijayan, O. G. Poluektov, T. Rajh, K. A. Gray, H. Y. He and P. Zapol, *J. Am. Chem. Soc.*, 2011, **133**, 3964.
24. J. Lee, D. C. Sorescu and X. Y. Deng, *J. Am. Chem. Soc.*, 2011, **133**, 10066.
25. S. J. Tan, Y. Zhao, J. Zhao, Z. Wang, C. X. Ma, A. D. Zhao, B. Wang, Y. Luo, J. L. Yang and J. G. Hou, *Phys. Rev. B*, 2011, **84**, 155418.
26. V. P. Indrakanti, H. H. Schobert and J. D. Kubicki, *Energy Fuels*, 2009, **23**, 5247.
27. D. C. Sorescu, W. A. Al-Saidi and K. D. Jordan, *J. Chem. Phys.*, 2011, **135**, 124701.
28. K. Xie, N. Umezawa, N. Zhang, P. Reunchan, Y. Zhang and J. Ye, *Energy Environ. Sci.*, 2011, **4**, 4211.
29. D. C. Sorescu, J. Lee, W. A. Al-Saidi and K. D. Jordan, *J. Chem. Phys.*, 2012, **137**, 074704.
30. G. C. Xi, S. X. Ouyang, P. Li, J. H. Ye, Q. Ma, N. Su, H. Bai and C. Wang, *Angew. Chem., Int. Ed.*, 2012, **51**, 2395.
31. L. G. Wang, S. J. Pennycook and S. T. Pantelides, *Phys. Rev. Lett.*, 2002, **89**, 075506.

32. Z. Goren, I. Willner, A. J. Nelson and A. J. Frank, *J. Phys. Chem.*, 1990, **94**, 3784.
33. M. Anpo and K. Chiba, *J. Mol. Catal.*, 1992, **74**, 207.
34. O. Ishitani, C. Inoue, Y. Suzuki and T. Ibusuki, *J. Photochem. Photobiol. A*, 1993, **72**, 269.
35. H. Inoue, T. Matsuyama, B. J. Liu, T. Sakata, H. Mori and H. Yoneyama, *Chem. Lett.*, 1994, 653.
36. F. Solymosi and I. Tombacz, *Catal. Lett.*, 1994, **27**, 61.
37. H. Yamashita, H. Nishiguchi, N. Kamada, M. Anpo, Y. Teraoka, H. Hatano, S. Ehara, K. Kikui, L. Palmisano, A. Sclafani, M. Schiavello and M. A. Fox, *Res. Chem. Intermed.*, 1994, **20**, 815.
38. M. Anpo, H. Yamashita, Y. Ichihashi and S. Ehara, *J. Electroanal. Chem.*, 1995, **396**, 21.
39. F. Saladin, L. Forss and I. Kamber, *J. Chem. Soc., Chem. Commun.*, 1995, 533.
40. S. Yamagata, M. Nishijo, N. Murao, S. Ohta and I. Mizoguchi, *Zeolites*, 1995, **15**, 490.
41. T. Mizuno, K. Adachi, K. Ohta and A. Saji, *J. Photochem. Photobiol. A*, 1996, **98**, 87.
42. M. Anpo, H. Yamashita, Y. Ichihashi, Y. Fujii and M. Honda, *J. Phys. Chem. B*, 1997, **101**, 2632.
43. S. Kaneco, H. Kurimoto, K. Ohta, T. Mizuno and A. Saji, *J. Photochem. Photobiol. A*, 1997, **109**, 59.
44. B. J. Liu, T. Torimoto, H. Matsumoto and H. Yoneyama, *J. Photochem. Photobiol. A*, 1997, **108**, 187.
45. F. Saladin and I. Alxneit, *J. Chem. Soc., Faraday Trans.*, 1997, **93**, 4159.
46. M. Anpo, H. Yamashita, K. Ikeue, Y. Fujii, S. G. Zhang, Y. Ichihashi, D. R. Park, Y. Suzuki, K. Koyano and T. Tatsumi, *Catal. Today*, 1998, **44**, 327.
47. S. Kaneco, Y. Shimizu, K. Ohta and T. Mizuno, *J. Photochem. Photobiol. A*, 1998, **115**, 223.
48. B. J. Liu, T. Torimoto and H. Yoneyama, *J. Photochem. Photobiol. A*, 1998, **115**, 227.
49. H. Yamashita, Y. Fujii, Y. Ichihashi, S. G. Zhang, K. Ikeue, D. R. Park, K. Koyano, T. Tatsumi and M. Anpo, *Catal. Today*, 1998, **45**, 221.
50. K. Ikeue, H. Yamashita and M. Anpo, *Chem. Lett.*, 1999, 1135.
51. S. Kaneco, H. Kurimoto, Y. Shimizu, K. Ohta and T. Mizuno, *Energy*, 1999, **24**, 21.
52. Y. Kohno, H. Hayashi, S. Takenaka, T. Tanaka, T. Funabiki and S. Yoshida, *J. Photochem. Photobiol., A*, 1999, **126**, 117.
53. M. Subrahmanyam, S. Kaneco and N. Alonso-Vante, *Appl. Catal., B*, 1999, **23**, 169.
54. K. Ikeue, H. Yamashita, M. Anpo and T. Takewaki, *J. Phys. Chem. B*, 2001, **105**, 8350.
55. K. Ikeue, H. Yamashita, T. Takewaki, M. E. Davis and M. Anpo, *J. Synchrotron Radiat.*, 2001, **8**, 602.

56. Y. Kohno, T. Yamamoto, T. Tanaka and T. Funabiki, *J. Mol. Catal. A: Chem.*, 2001, **175**, 173.
57. T. F. Xie, D. J. Wang, L. J. Zhu, T. J. Li and Y. J. Xu, *Mater. Chem. Phys.*, 2001, **70**, 103.
58. K. Ikeue, S. Nozaki, M. Ogawa and M. Anpo, *Catal. Lett.*, 2002, **80**, 111.
59. I. Keita, S. Nozaki, M. Ogawa and M. Anpo, *Catal. Today*, 2002, **74**, 241.
60. I. H. Tseng, W. C. Chang and J. C. S. Wu, *Appl. Catal., B*, 2002, **37**, 37.
61. H. Yamashita, K. Ikeue, T. Takewaki and M. Anpo, *Top. Catal.*, 2002, **18**, 95.
62. Y. Shioya, K. Ikeue, M. Ogawa and M. Anpo, *Appl. Catal., A*, 2003, **254**, 251.
63. G. R. Dey, A. D. Belapurkar and K. Kishore, *J. Photochem. Photobiol., A*, 2004, **163**, 503.
64. Y. Ku, W. H. Lee and W. Y. Wang, *J. Mol. Catal. A: Chem.*, 2004, **212**, 191.
65. P. Pathak, M. J. Meziani, Y. Li, L. T. Cureton and Y. P. Sun, *Chem. Commun.*, 2004, 1234.
66. I. H. Tseng and J. C. S. Wu, *Catal. Today*, 2004, **97**, 113.
67. I. H. Tseng, J. C. S. Wu and H. Y. Chou, *J. Catal.*, 2004, **221**, 432.
68. J. S. Hwang, J. S. Chang, S. E. Park, K. Ikeue and M. Anpo, *Top. Catal.*, 2005, **35**, 311.
69. P. Pathak, M. J. Meziani, L. Castillo and Y. P. Sun, *Green Chem.*, 2005, **7**, 667.
70. J. C. S. Wu and H. M. Lin, *Int. J. Photoenergy*, 2005, **7**, 115.
71. J. C. S. Wu, H.-M. Lin and C.-L. Lai, *Appl. Catal., A*, 2005, **296**, 194.
72. Y. Q. Liu, Y. Xu, Z. J. Li, X. P. Zhang, D. Wu and Y. H. Sun, *Acta Chim. Sin.*, 2006, **64**, 453.
73. G. R. Dey and K. K. Pushpa, *Res. Chem. Intermed.*, 2007, **33**, 631.
74. C.-C. Lo, C.-H. Hung, C.-S. Yuan and J.-F. Wu, *Sol. Energy Mater. Sol. Cells*, 2007, **91**, 1765.
75. X. H. Xia, Z. H. Jia, Y. Yu, Y. Liang, Z. Wang and L. L. Ma, *Carbon*, 2007, **45**, 717.
76. T. V. Nguyen and J. C. S. Wu, *Sol. Energy Mater. Sol. Cells*, 2008, **92**, 864.
77. T.-V. Nguyen and J. C. S. Wu, *Appl. Catal., A*, 2008, **335**, 112.
78. J. C. S. Wu, T. H. Wu, T. C. Chu, H. J. Huang and D. P. Tsai, *Top. Catal.*, 2008, **47**, 131.
79. L. Chen, M. E. Graham, G. H. Li, D. R. Gentner, N. M. Dimitrijevic and K. A. Gray, *Thin Solid Films*, 2009, **517**, 5641.
80. K. Koci, L. Obalova, L. Matejova, D. Placha, Z. Lacny, J. Jirkovsky and O. Solcova, *Appl. Catal., B*, 2009, **89**, 494.
81. O. K. Varghese, M. Paulose, T. J. LaTempa and C. A. Grimes, *Nano Lett.*, 2009, **9**, 731.
82. H. C. Yang, H. Y. Lin, Y. S. Chien, J. C. S. Wu and H. H. Wu, *Catal. Lett.*, 2009, **131**, 381.
83. L. F. Cueto, G. T. Martinez, G. Zavala and E. M. Sanchez, *J. Nano Res.*, 2010, **9**, 89.

84. Y. Li, W. N. Wang, Z. L. Zhan, M. H. Woo, C. Y. Wu and P. Biswas, *Appl. Catal., B*, 2010, **100**, 386.
85. K. Nalepa, J. Goralski, M. I. Szynkowska and J. Rynkowski, *Przem. Chem.*, 2010, **89**, 500.
86. X. Feng, J. D. Sloppy, T. J. LaTempa, M. Paulose, S. Komarneni, N. Bao and C. A. Grimes, *J. Mater. Chem.*, 2011, **21**, 13429.
87. K. Koci, V. Matejka, P. Kovar, Z. Lacny and L. Obalova, *Catal. Today*, 2011, **161**, 105.
88. Y. T. Liang, B. K. Vijayan, K. A. Gray and M. C. Hersam, *Nano Lett.*, 2011, **11**, 2865.
89. J. Pan, X. Wu, L. Z. Wang, G. Liu, G. Q. Lub and H. M. Cheng, *Chem. Commun.*, 2011, **47**, 8361.
90. S. Y. Qin, F. Xin, Y. D. Liu, X. H. Yin and W. Ma, *J. Colloid Interface Sci.*, 2011, **356**, 257.
91. K. S. Raja, Y. R. Smith, N. Kondamudi, A. Manivannan, M. Misra and V. Subramanian, *Electrochem. Solid-State Lett.*, 2011, **14**, F5.
92. B. Srinivas, B. Shubhamangala, K. Lalitha, P. A. K. Reddy, V. D. Kumari, M. Subrahmanyam and B. R. De, *Photochem. Photobiol.*, 2011, **87**, 995.
93. W.-N. Wang, J. Park and P. Biswas, *Catal. Sci. Technol.*, 2011, **1**, 593.
94. G. C. Xi, S. X. Ouyang and J. H. Ye, *Chem.–Eur. J.*, 2011, **17**, 9057.
95. C. C. Yang, J. Vernimmen, V. Meynen, P. Cool and G. Mul, *J. Catal.*, 2011, **284**, 1.
96. T. Yui, A. Kan, C. Saitoh, K. Koike, T. Ibusuki and O. Ishitani, *ACS Appl. Mater. Interfaces*, 2011, **3**, 2594.
97. A. Cybula, M. Klein, A. Zielinska-Jurek, M. Janczarek and A. Zaleska, *Physicochem. Probl.*, 2012, **48**, 159.
98. W. Jiao, L. Z. Wang, G. Liu, G. Q. Lu and H. M. Cheng, *ACS Catal.*, 2012, **2**, 1854.
99. W. Kim, T. Seok and W. Choi, *Energy Environ. Sci.*, 2012, **5**, 6066.
100. D. Liu, Y. Fernandez, O. Ola, S. Mackintosh, M. Maroto-Valer, C. M. A. Parlett, A. F. Lee and J. C. S. Wu, *Catal. Commun.*, 2012, **25**, 78.
101. J. Z. Y. Tan, Y. Fernandez, D. Liu, M. Maroto-Valer, J. C. Bian and X. W. Zhang, *Chem. Phys. Lett.*, 2012, **531**, 149.
102. W. G. Tu, Y. Zhou, Q. Liu, Z. P. Tian, J. Gao, X. Y. Chen, H. T. Zhang, J. G. Liu and Z. G. Zou, *Adv. Funct. Mater.*, 2012, **22**, 1215.
103. P. Q. Wang, Y. Bai, J. Y. Liu, Z. Fan and Y. Q. Hu, *Catal. Commun.*, 2012, **29**, 185.
104. W. N. Wang, W. J. An, B. Ramalingam, S. Mukherjee, D. M. Niedzwiedzki, S. Gangopadhyay and P. Biswas, *J. Am. Chem. Soc.*, 2012, **134**, 11276.
105. X. J. Zhang, F. Han, B. Shi, S. Farsinezhad, G. P. Dechaine and K. Shankar, *Angew. Chem., Int. Ed.*, 2012, **51**, 12732.
106. C. Y. Zhao, A. Kroll, H. L. Zhao, Q. Y. Zhang and Y. Li, *Int. J. Hydrogen Energy*, 2012, **37**, 9967.
107. M. Hussain, P. Akhter, N. Russo and G. Saracco, *Catal. Commun.*, 2013, **36**, 58.

108. L. Liu, F. Gao, H. Zhao and Y. Li, *Appl. Catal., B*, 2013, **134–135**, 349.
109. W. G. Tu, Y. Zhou, Q. Liu, S. C. Yan, S. S. Bao, X. Y. Wang, M. Xiao and Z. G. Zou, *Adv. Funct. Mater.*, 2013, **23**, 1743.
110. Y. G. Wang, B. Li, C. L. Zhang, L. F. Cui, S. F. Kang, X. Li and L. H. Zhou, *Appl. Catal., B*, 2013, **130**, 277.
111. H. Xu, S. X. Ouyang, P. Li, T. Kako and J. H. Ye, *ACS Appl. Mater. Interfaces*, 2013, **5**, 1348.
112. Q. G. Zhai, S. J. Xie, W. Q. Fan, Q. H. Zhang, Y. Wang, W. P. Deng and Y. Wang, *Angew. Chem., Int. Ed.*, 2013, **52**, 5776.
113. C. L. Zhang, Q. Y. Zhang, S. F. Kang, B. Li, X. Li and Y. G. Wang, *ECS Solid State Lett.*, 2013, **2**, M49.
114. Slamet, H. W. Nasution, E. Purnama, S. Kosela and J. Gunlazuardi, *Catal. Commun.*, 2005, **6**, 313.
115. N. Sasirekha, S. J. S. Basha and K. Shanthi, *Appl. Catal., B*, 2006, **62**, 169.
116. S. H. Liu, Z. H. Zhao and Z. Z. Wang, *Photochem. Photobiol. Sci.*, 2007, **6**, 695.
117. O. Ozcan, F. Yukruk, E. U. Akkaya and D. Uner, *Top. Catal.*, 2007, **44**, 523.
118. O. Ozcan, F. Yukruk, E. U. Akkaya and D. Uner, *Appl. Catal., B*, 2007, **71**, 291.
119. T. V. Nguyen, J. C. S. Wu and C. H. Chiou, *Catal. Commun.*, 2008, **9**, 2073.
120. Z. H. Zhao, J. M. Fan, S. H. Liu and Z. Z. Wang, *Chem. Eng. J.*, 2009, **151**, 134.
121. Z. H. Zhao, J. M. Fan, M. M. Xie and Z. Z. Wang, *J. Cleaner Prod.*, 2009, **17**, 1025.
122. K. Koci, K. Mateju, L. Obalova, S. Krejcikova, Z. Lacny, D. Placha, L. Capek, A. Hospodkova and O. Solcova, *Appl. Catal., B*, 2010, **96**, 239.
123. C. J. Wang, R. L. Thompson, J. Baltrus and C. Matranga, *J. Phys. Chem. Lett.*, 2010, **1**, 48.
124. T. W. Woolerton, S. Sheard, E. Reisner, E. Pierce, S. W. Ragsdale and F. A. Armstrong, *J. Am. Chem. Soc.*, 2010, **132**, 2132.
125. M. Abou Asi, C. He, M. H. Su, D. H. Xia, L. Lin, H. Q. Deng, Y. Xiong, R. L. Qiu and X. Z. Li, *Catal. Today*, 2011, **175**, 256.
126. J. Fan, E. Z. Liu, L. Tian, X. Y. Hu, Q. He and T. Sun, *J. Environ. Eng.-ASCE*, 2011, **137**, 171.
127. W. B. Hou, W. H. Hung, P. Pavaskar, A. Goeppert, M. Aykol and S. B. Cronin, *ACS Catal.*, 2011, **1**, 929.
128. D. M. Luo, Y. Bi, W. Kan, N. Zhang and S. G. Hong, *J. Mol. Struct.*, 2011, **994**, 325.
129. C. J. Wang, R. L. Thompson, P. Ohodnicki, J. Baltrus and C. Matranga, *J. Mater. Chem.*, 2011, **21**, 13452.
130. T. W. Woolerton, S. Sheard, E. Pierce, S. W. Ragsdale and F. A. Armstrong, *Energy Environ. Sci.*, 2011, **4**, 2393.
131. Q. Y. Zhang, Y. Li, E. A. Ackerman, M. Gajdardziska-Josifovska and H. L. Li, *Appl. Catal., A*, 2011, **400**, 195.
132. S.-I. In, D. D. Vaughn and R. E. Schaak, *Angew. Chem., Int. Ed.*, 2012, **51**, 3915.

133. S. Krejcikova, L. Matejova, K. Koci, L. Obalova, Z. Matej, L. Capek and O. Solcova, *Appl. Catal., B*, 2012, **111**, 119.
134. X. Li, H. L. Liu, D. L. Luo, J. T. Li, Y. Huang, H. L. Li, Y. P. Fang, Y. H. Xu and L. Zhu, *Chem. Eng. J.*, 2012, **180**, 151.
135. X. K. Li, Z. J. Zhuang, W. Li and H. Q. Pan, *Appl. Catal., A*, 2012, **429**, 31.
136. L. J. Liu, C. Y. Zhao and Y. Li, *J. Phys. Chem. C*, 2012, **116**, 7904.
137. L. J. Liu, H. L. Zhao, J. M. Andino and Y. Li, *ACS Catal.*, 2012, **2**, 1817.
138. P. L. Richardson, M. L. N. Perdigoto, W. Wang and R. J. G. Lopes, *Appl. Catal., B*, 2012, **126**, 200.
139. Q. D. Truong, T. H. Le, J. Y. Liu, C. C. Chung and Y. C. Ling, *Appl. Catal., A*, 2012, **437**, 28.
140. Q. D. Truong, J. Y. Liu, C. C. Chung and Y. C. Ling, *Catal. Commun.*, 2012, **19**, 85.
141. Q. Wang, W. Wu, J. F. Chen, G. W. Chu, K. Ma and H. K. Zou, *Colloids Surf., A*, 2012, **409**, 118.
142. Y. J. Yuan, Z. T. Yu, J. Y. Zhang and Z. G. Zou, *Dalton Trans.*, 2012, **41**, 9594.
143. Q. Y. Zhang, T. T. Gao, J. M. Andino and Y. Li, *Appl. Catal., B*, 2012, **123**, 257.
144. C. Y. Zhao, L. J. Liu, Q. Y. Zhang, J. Wang and Y. Li, *Catal. Sci. Technol.*, 2012, **2**, 2558.
145. W. J. Ong, M. M. Gui, S. P. Chai and A. R. Mohamed, *RSC Adv.*, 2013, **3**, 4505.
146. G. Qin, Y. Zhang, X. Ke, X. Tong, Z. Sun, M. Liang and S. Xue, *Appl. Catal., B*, 2013, **129**, 599.
147. P. L. Richardson, M. L. N. Perdigoto, W. Wang and R. J. G. Lopes, *Appl. Catal., B*, 2013, **132–133**, 408.
148. Y. S. Liao, S. W. Cao, Y. P. Yuan, Q. Gu, Z. Y. Zhang and C. Xue, *Chem.–Eur. J.*, 2014, **20**, 10220.
149. X. Meng, S. Ouyang, T. Kako, P. Li, Q. Yu, T. Wang and J. Ye, *Chem. Commun.*, 2014, **50**, 11517.
150. T. Wang, X. Meng, P. Li, S. Ouyang, K. Chang, G. Liu, Z. Mei and J. Ye, *Nano Energy*, 2014, **9**, 50.
151. H. Xu, S. X. Ouyang, L. Q. Liu, D. F. Wang, T. Kako and J. H. Ye, *Nanotechnology*, 2014, **25**, 165402, paper.
152. J. C. Hemminger, R. Carr and G. A. Somorjai, *Chem. Phys. Lett.*, 1978, **57**, 100.
153. D. D. Sui, X. H. Yin, H. Z. Dong, S. Y. Qin, J. S. Chen and W. L. Jiang, *Catal. Lett.*, 2012, **142**, 1202.
154. H. Zhou, J. J. Guo, P. Li, T. X. Fan, D. Zhang and J. H. Ye, *Sci. Rep.*, 2013, **3**, 075506.
155. M. Ulman, B. Aurianblajeni and M. Halmann, *Isr. J. Chem.*, 1982, **22**, 177.
156. G. Q. Guan, T. Kida, T. Harada, M. Isayama and A. Yoshida, *Appl. Catal., A*, 2003, **249**, 11.
157. G. Q. Guan, T. Kida and A. Yoshida, *Appl. Catal., B*, 2003, **41**, 387.
158. K. Iizuka, T. Wato, Y. Miseki, K. Saito and A. Kudo, *J. Am. Chem. Soc.*, 2011, **133**, 20863.

159. Y. Y. Liu, B. B. Huang, Y. Dai, X. Y. Zhang, X. Y. Qin, M. H. Jiang and M. H. Whangbo, *Catal. Commun.*, 2009, **11**, 210.
160. P. Li, Y. Zhou, W. G. Tu, Q. Liu, S. C. Yan and Z. G. Zou, *ChemPlusChem*, 2013, **78**, 274.
161. K. Sayama and H. Arakawa, *J. Phys. Chem.*, 1993, **97**, 531.
162. Y. Kohno, T. Tanaka, T. Funabiki and S. Yoshida, *Chem. Commun.*, 1997, 841.
163. Y. Kohno, T. Tanaka, T. Funabiki and S. Yoshida, *J. Chem. Soc., Faraday Trans.*, 1998, **94**, 1875.
164. Y. Kohno, T. Tanaka, T. Funabiki and S. Yoshida, *Phys. Chem. Chem. Phys.*, 2000, **2**, 2635.
165. X. K. Li, W. Li, Z. J. Zhuang, Y. S. Zhong, Q. Li and L. Y. Wang, *J. Phys. Chem. C*, 2012, **116**, 16047.
166. X. K. Li, H. Q. Pan, W. Li and Z. J. Zhuang, *Appl. Catal., A*, 2012, **413**, 103.
167. D. S. Lee, H. J. Chen and Y. W. Chen, *J. Phys. Chem. Solids*, 2012, **73**, 661.
168. H. F. Shi, T. Z. Wang, J. Chen, C. Zhu, J. H. Ye and Z. G. Zou, *Catal. Lett.*, 2011, **141**, 525.
169. M. Stock and S. Dunn, *Ferroelectrics*, 2011, **419**, 9.
170. P. Li, S. X. Ouyang, G. C. Xi, T. Kako and J. H. Ye, *J. Phys. Chem. C*, 2012, **116**, 7621.
171. H. Shi and Z. Zou, *J. Phys. Chem. Solids*, 2012, **73**, 788.
172. P. Li, S. X. Ouyang, Y. J. Zhang, T. Kako and J. H. Ye, *J. Mater. Chem. A*, 2013, **1**, 1185.
173. P. Li, H. Xu, L. Liu, T. Kako, N. Umezawa, H. Abe and J. Ye, *J. Mater. Chem. A*, 2014, **2**, 5606.
174. Y. Z. P. Li, W. G. Tu, R. Wang, C. F. Zhang, Q. Liu, H. J. Li, Z. D. Li, H. Dai, J. J. Wang, S. C. Yan and Z. G. Zou, *CrystEngComm*, 2013, **15**, 9855.
175. S. Sato, T. Morikawa, S. Saeki, T. Kajino and T. Motohiro, *Angew. Chem., Int. Ed.*, 2010, **49**, 5101.
176. T. M. Suzuki, H. Tanaka, T. Morikawa, M. Iwaki, S. Sato, S. Saeki, M. Inoue, T. Kajino and T. Motohiro, *Chem. Commun.*, 2011, **47**, 8673.
177. P. W. Pan and Y. W. Chen, *Catal. Commun.*, 2007, **8**, 1546.
178. H. C. Chen, H. C. Chou, J. C. S. Wu and H. Y. Lin, *J. Mater. Res.*, 2008, **23**, 1364.
179. Z.-Y. Wang, H.-C. Chou, J. C. S. Wu, D. P. Tsai and G. Mul, *Appl. Catal., A*, 2010, **380**, 172.
180. P. Y. Liou, S. C. Chen, J. C. S. Wu, D. Liu, S. Mackintosh, M. Maroto-Valer and R. Linforth, *Energy Environ. Sci.*, 2011, **4**, 1487.
181. C. W. Tsai, H. M. Chen, R. S. Liu, K. Asakura and T. S. Chan, *J. Phys. Chem. C*, 2011, **115**, 10180.
182. K. Teramura, S.-i. Okuoka, H. Tsuneoka, T. Shishido and T. Tanaka, *Appl. Catal., B*, 2010, **96**, 565.
183. X. Y. Chen, Y. Zhou, Q. Liu, Z. D. Li, J. G. Liu and Z. G. Zou, *ACS Appl. Mater. Interfaces*, 2012, **4**, 3372.

184. Y. P. Xie, G. Liu, L. C. Yin and H. M. Cheng, *J. Mater. Chem.*, 2012, **22**, 6746.
185. Y. Zhou, Z. P. Tian, Z. Y. Zhao, Q. Liu, J. H. Kou, X. Y. Chen, J. Gao, S. C. Yan and Z. G. Zou, *ACS Appl. Mater. Interfaces*, 2011, **3**, 3594.
186. H. F. Cheng, B. B. Huang, Y. Y. Liu, Z. Y. Wang, X. Y. Qin, X. Y. Zhang and Y. Dai, *Chem. Commun.*, 2012, **48**, 9729.
187. A. Kudo and Y. Miseki, *Chem. Soc. Rev.*, 2009, **38**, 253.
188. J. J. Guo, S. X. Ouyang, T. Kako and J. H. Ye, *Appl. Surf. Sci.*, 2013, **280**, 418.
189. H. Tsuneoka, K. Teramura, T. Shishido and T. Tanaka, *J. Phys. Chem. C*, 2010, **114**, 8892.
190. H. A. Park, J. H. Choi, K. M. Choi, D. K. Lee and J. K. Kang, *J. Mater. Chem.*, 2012, **22**, 5304.
191. K. Teramura, H. Tsuneoka, T. Shishido and T. Tanaka, *Chem. Phys. Lett.*, 2008, **467**, 191.
192. S. C. Yan, S. X. Ouyang, J. Gao, M. Yang, J. Y. Feng, X. X. Fan, L. J. Wan, Z. S. Li, J. H. Ye, Y. Zhou and Z. G. Zou, *Angew. Chem., Int. Ed.*, 2010, **49**, 6400.
193. S. C. Yan, J. J. Wang, H. L. Gao, N. Y. Wang, H. Yu, Z. S. Li, Y. Zhou and Z. G. Zou, *Adv. Funct. Mater.*, 2013, **23**, 758.
194. J. W. Lekse, M. K. Underwood, J. P. Lewis and C. Matranga, *J. Phys. Chem. C*, 2012, **116**, 1865.
195. Z. D. Li, Y. Zhou, J. Y. Zhang, W. G. Tu, Q. Liu, T. Yu and Z. G. Zou, *Cryst. Growth Des.*, 2012, **12**, 1476.
196. Q. Liu, Y. Zhou, J. H. Kou, X. Y. Chen, Z. P. Tian, J. Gao, S. C. Yan and Z. G. Zou, *J. Am. Chem. Soc.*, 2010, **132**, 14385.
197. S. C. Yan, L. J. Wan, Z. S. Li and Z. G. Zou, *Chem. Commun.*, 2011, **47**, 5632.
198. N. Zhang, S. X. Ouyang, P. Li, Y. J. Zhang, G. C. Xi, T. Kako and J. H. Ye, *Chem. Commun.*, 2011, **47**, 2041.
199. Q. Liu, Z. X. Low, L. X. Li, A. Razmjou, K. Wang, J. F. Yao and H. T. Wang, *J. Mater. Chem. A*, 2013, **1**, 11563.
200. Q. Liu, Y. Zhou, Y. Ma and Z. G. Zou, *RSC Adv.*, 2012, **2**, 3247.
201. Y. Inoue, *Energy Environ. Sci.*, 2009, **2**, 364.
202. J. Sato, H. Kobayashi, K. Ikarashi, N. Saito, H. Nishiyama and Y. Inoue, *J. Phys. Chem. B*, 2004, **108**, 4369.
203. K. Ikarashi, J. Sato, H. Kobayashi, N. Saito, H. Nishiyama and Y. Inoue, *J. Phys. Chem. B*, 2002, **106**, 9048.
204. B. R. Eggins, J. T. S. Irvine, E. P. Murphy and J. Grimshaw, *J. Chem. Soc., Chem. Commun.*, 1988, 1123.
205. M. Kanemoto, T. Shiragami, C. J. Pac and S. Yanagida, *J. Phys. Chem.*, 1992, **96**, 3521.
206. H. Inoue, H. Moriwaki, K. Maeda and H. Yoneyama, *J. Photochem. Photobiol., A*, 1995, **86**, 191.
207. H. Fujiwara, H. Hosokawa, K. Murakoshi, Y. Wada, S. Yanagida, T. Okada and H. Kobayashi, *J. Phys. Chem. B*, 1997, **101**, 8270.

208. P. Johne and H. Kisch, *J. Photochem. Photobiol., A.*, 1997, **111**, 223.
209. B. R. Eggins, P. K. J. Robertson, E. P. Murphy, E. Woods and J. T. S. Irvine, *J. Photochem. Photobiol., A.*, 1998, **118**, 31.
210. H. Fujiwara, H. Hosokawa, K. Murakoshi, Y. Wada and S. Yanagida, *Langmuir*, 1998, **14**, 5154.
211. B. J. Liu, T. Torimoto and H. Yoneyama, *J. Photochem. Photobiol., A*, 1998, **113**, 93.
212. H. Kisch and P. Lutz, *Photochem. Photobiol. Sci.*, 2002, **1**, 240.
213. P. Praus, O. Kozak, K. Koci, A. Panacek and R. Dvorsky, *J. Colloid Interface Sci.*, 2011, **360**, 574.
214. Y. S. Chaudhary, T. W. Woolerton, C. S. Allen, J. H. Warner, E. Pierce, S. W. Ragsdale and F. A. Armstrong, *Chem. Commun.*, 2012, **48**, 58.
215. J.-Y. Liu, B. Garg and Y.-C. Ling, *Green Chem.*, 2011, **13**, 2029.
216. T. Arai, S. Tajima, S. Sato, K. Uemura, T. Morikawa and T. Kajino, *Chem. Commun.*, 2011, **47**, 12664.
217. T. Arai, S. Sato, K. Uemura, T. Morikawa, T. Kajino and T. Motohiro, *Chem. Commun.*, 2010, **46**, 6944.
218. S. Sato, T. Arai, T. Morikawa, K. Uemura, T. M. Suzuki, H. Tanaka and T. Kajino, *J. Am. Chem. Soc.*, 2011, **133**, 15240.
219. T. Arai, S. Sato, T. Kajino and T. Morikawa, *Energy Environ. Sci.*, 2013, **6**, 1274.
220. E. E. Barton, D. M. Rampulla and A. B. Bocarsly, *J. Am. Chem. Soc.*, 2008, **130**, 6342.
221. M. Halmann, *Nature*, 1978, **275**, 115.
222. H. L. Li, Y. G. Lei, Y. Huang, Y. P. Fang, Y. H. Xu, L. Zhu and X. Li, *J. Nat. Gas Chem.*, 2011, **20**, 145.
223. M. A. Gondal, M. A. Ali, M. A. Dastageer and X. F. Chang, *Catal. Lett.*, 2013, **143**, 108.
224. N. Ahmed, Y. Shibata, T. Taniguchi and Y. Izumi, *J. Catal.*, 2011, **279**, 123.
225. K. Teramura, S. Iguchi, Y. Mizuno, T. Shishido and T. Tanaka, *Angew. Chem., Int. Ed.*, 2012, **51**, 8008.
226. N. Ahmed, M. Morikawa and Y. Izumi, *Catal. Today*, 2012, **185**, 263.
227. G. H. Dong and L. Z. Zhang, *J. Mater. Chem.*, 2012, **22**, 1160.
228. J. Mao, T. Peng, X. Zhang, K. Li, L. Ye and L. Zan, *Catal. Sci. Technol.*, 2013, **3**, 1253.
229. L. Cao, S. Sahu, P. Anilkumar, C. E. Bunker, J. A. Xu, K. A. S. Fernando, P. Wang, E. A. Guliants, K. N. Tackett and Y. P. Sun, *J. Am. Chem. Soc.*, 2011, **133**, 4754.
230. H. Zhou, P. Li, J. Guo, R. Yan, T. Fan, D. Zhang and J. Ye, *Nanoscale*, 2015, **7**, 113.
231. N. Zhang, S. X. Ouyang, T. Kako and J. H. Ye, *Chem. Commun.*, 2012, **48**, 1269.
232. S. C. Yan, J. J. Wang, H. L. Gao, N. Y. Wang, H. Yu, Z. S. Li, Y. Zhou and Z. G. Zou, *Adv. Funct. Mater.*, 2013, **23**, 1839.
233. G. Liu, J. C. Yu, G. Q. Lu and H. M. Cheng, *Chem. Commun.*, 2011, **47**, 6763.

234. M. Lazzeri, A. Vittadini and A. Selloni, *Phys. Rev. B.*, 2001, **63**, 155409.
235. M. Lazzeri, A. Vittadini and A. Selloni, *Phys. Rev. B.*, 2002, **65**, 119901.
236. H. G. Yang, C. H. Sun, S. Z. Qiao, J. Zou, G. Liu, S. C. Smith, H. M. Cheng and G. Q. Lu, *Nature*, 2008, **453**, 638.
237. H. Yamashita, N. Kamada, H. He, K. Tanaka, S. Ehara and M. Anpo, *Chem. Lett.*, 1994, 855.
238. M. Anpo, H. Yamashita, Y. Ichihashi and S. Ehara, *J. Electroanal. Chem.*, 1995, **396**, 21.
239. A. Ignatchenko, D. G. Nealon, R. Dushane and K. Humphries, *J. Mol. Catal. A: Chem.*, 2006, **256**, 57.
240. V. P. Indrakanti, J. D. Kubicki and H. H. Schobert, *Energy Fuels*, 2008, **22**, 2611.
241. Y. S. Liao, S. W. Cao, Y. P. Yuan, Q. Gu, Z. Y. Zhang and C. Xue, *Chem.–Eur. J.*, 2014, **20**, 10220.
242. W. Choi, A. Termin and M. R. Hoffmann, *Angew. Chem.*, 1994, **106**, 1148.
243. K. Maeda, K. Teramura, D. L. Lu, T. Takata, N. Saito, Y. Inoue and K. Domen, *Nature*, 2006, **440**, 295.
244. Q. Liu, Y. Zhou, Z. P. Tian, X. Y. Chen, J. Gao and Z. G. Zou, *J. Mater. Chem.*, 2012, **22**, 2033.
245. K. Maeda and K. Domen, *J. Phys. Chem. Lett.*, 2010, **1**, 2655.
246. D. Wang, T. Hisatomi, T. Takata, C. Pan, M. Katayama, J. Kubota and K. Domen, *Angew. Chem., Int. Ed.*, 2013, **52**, 11252.
247. W. Tu, Y. Zhou and Z. Zou, *Adv. Funct. Mater.*, 2013, **23**, 4996.
248. K. Sekizawa, K. Maeda, K. Domen, K. Koike and O. Ishitani, *J. Am. Chem. Soc.*, 2013, **135**, 4596.